

Comparison of Two Ultra-Widefield Cameras With High Image Resolution and Wider View for Identifying Diabetic Retinopathy Lesions

Rehana Khan¹, Sundaresan Raman^{1,2}, Sri Krishna M. Karamchetti², Sangeetha Srinivasan³, Abhishek Sharma^{1,4}, Janani Surya¹, Muna Bhende¹, Kim Ramasamy⁵, Aditya Verma¹, and Rajiv Raman¹

¹ Shri Bhagwan Mahavir Vitreoretinal Services, Sankara Nethralaya, Chennai, Tamil Nadu, India

² Birla Institute of Technology and Science, Pilani, Rajasthan, India

³ Vision Research Foundation, Chennai, Tamil Nadu, India

⁴ Michigan State University College of Human Medicine, East Lansing, MI, USA

⁵ Retina and Vitreous Services, Aravind Eye Care System, Madurai, Tamil Nadu, India

Correspondence: Rajiv Raman, Shri Bhagwan Mahavir Vitreoretinal Services, Sankara Nethralaya, 18 College Road, Chennai 600006, Tamil Nadu, India. e-mail: rajivpgraman@gmail.com

Received: April 20, 2021

Accepted: September 10, 2021

Published: October 6, 2021

Keywords: diabetes mellitus; retinopathy; ultra-widefield; Optos; Clarus

Citation: Khan R, Raman S, Karamchetti SKM, Srinivasan S, Sharma A, Surya J, Bhende M, Ramasamy K, Verma A, Raman R. Comparison of two ultra-widefield cameras with high image resolution and wider view for identifying diabetic retinopathy lesions. *Transl Vis Sci Technol.* 2021;10(12):9, <https://doi.org/10.1167/tvst.10.12.9>

Purpose: To compare the effectiveness of the Optos P200dTx and Zeiss Clarus 500 fundus cameras in detecting diabetic retinopathy (DR) lesions.

Methods: A cross-sectional study was conducted among 243 patients with clinically diagnosed diabetes mellitus who were referred for an eye examination from two tertiary eye care centers in Chennai, India. Patients underwent DR screening based on mydriatic fundal images acquired by both fundal cameras. Fundal images from the two separate devices for each eye were compared based on accurately identified pathological retinal lesions with respect to type and location.

Results: When studying lesions of the central retina, they were better identified by the Zeiss Clarus compared with the Optos P200dTx, with six out of eight being statistically significant ($P < 0.05$). However, lesions of the mid-peripheral retina and peripheral retina were better identified by the Optos P200dTx than the Zeiss Clarus, with three out of eight lesions and five out of eight lesions being statistically significant ($P < 0.05$), respectively. Based on the color and size of lesions, the Optos P200dTx had a higher chance (59.6%) of missing white lesions than did the Zeiss Clarus (17%) ($P < 0.0001$). Consequently, small- and medium-sized lesions were missed more by the Optos P200dTx (30.72% and 32.63%, respectively) than the Zeiss Clarus (22.3% and 19.30%, respectively).

Conclusions: The capability of detecting or missing a particular DR lesion among diabetics differed between the two cameras based on effective field of view, resolution, and the retinal zone being imaged.

Translational Relevance: The choice of which ultra-widefield camera to be used for screening DR can be based on the greater prevalence of central versus peripheral retinal lesions noted in the patient population seen in a clinical practice.

Introduction

Worldwide, diabetes is an important public health disease, more so in developing countries.¹ Fundus photography is now an established method of screening people with diabetes for diabetic retinopathy (DR).² Currently available retinal cameras have made

it possible to image the area of the retina as recommended by the Early Treatment Diabetic Retinopathy Study standard seven-field (S7F) protocol (75° of the fundus, which is approximately 34% of retinal surface) as a standardized screening strategy.³ Depending on the ethnicities, the distribution of peripheral lesions in diabetic retinopathy varies from 6% to 58%.⁴ However, studies have shown that identifying



previously undetected DR lesions in the peripheral fields might be better captured using ultra-widefield (UWF) imaging and may reveal a higher grade of DR than the S7F protocol.⁵ Such findings promote the utility of UWF cameras; however, which UWF camera to use based on the local clinical population has not been effectively studied, especially with regard to a primarily South Asian population.

The field of view covered by UWF has been defined by the Diabetic Retinopathy Clinical Research network to be at least 100° or greater.⁶ Accurate grading of DR involves identification of lesions and the extent of distribution of the lesions. To achieve this, a fundus camera with wider coverage and a high resolution is indispensable. The Optos P200dTx (Optos, Dunfermline, UK) and the Zeiss Clarus 500 (Carl Zeiss Meditec, Jena, Germany) are UWF fundus cameras that are utilized for UWF fundus imaging techniques. In a single capture, the Optos P200dTx, which is a non-contact, non-mydiatic camera, can capture up to a 200° field of view, whereas the Zeiss Clarus fundus camera obtains about 133°. That the Optos P200dTx is a pseudo-color imaging system has a direct bearing on the identification of lesions with different colors, as the Zeiss Clarus utilizes true colors, especially in DR.⁷ What influence having a wider field versus better resolution has on identifying lesions of DR in pigmented eyes remains yet to be known.

We aimed to compare the Optos P200dTx and Zeiss Clarus fundus cameras with respect to identification of specific DR retinal lesions and their distribution.

Methods

This cross-sectional study was conducted at two tertiary eye care institutions in India. All subjects were enrolled between January and November 2017. The study adhered to the tenets of the Declaration of Helsinki and was approved by the institutional review boards of both centers. Written informed consent was collected from all study participants.

A convenient sample of 243 consecutive patients with prior clinical diagnosis of type 2 diabetes mellitus who underwent retinal examinations were enrolled in the study. A total of 101 unilateral and 142 bilateral eyes were evaluated. Exclusion criteria were patients with dense cataract, posterior staphylomas, or overt media opacity; ungradable images due to poor quality; and an inability to capture the macula and peripheral retina due to patient's poor vision and non-cooperation. All patients underwent mydiatic fundus photography acquired using both the Optos P200dTx

and Zeiss Clarus to identify DR lesions and were later clinically diagnosed, in a double-blinded fashion with indirect ophthalmoscopy, as having DR, along with grading or the absence of DR.

Ground Truth Annotation Using SNAAnnotate

The lesions were annotated at the Sankara Nethralaya fundus photography reading center by trained graders using a custom web-based framework, SNAAnnotate. This framework was developed using Python and features the option of manual marking of lesions and labeling them. Eight types of lesions were considered for annotation to generate the ground truth: microaneurysm (MA), retinal hemorrhage (RH), hard exudate (HE), cotton wool spot (CWS), neovascularization of disc (NVD), neovascularization elsewhere (NVE), subhyaloid hemorrhage (SHH), and vitreous hemorrhage (VH). For each of the lesions, the grader could choose specific coordinate locations or points on an image or regions marked by circles indicating the extent or concentration of a lesion in a region, as shown in Figure 1. Three circular regions with increasing sizes (i.e., small, medium, and large) were considered for analysis in addition to point-type lesions, as illustrated in Figure 1. In our study, based on the size of different lesions, we employed points for MA, small regions for CWS and VH, and a point or small or medium regions for HE, RH, NVE, NVD, and SHH. The grading of each image was performed by 10 independent observers in a masked manner utilizing unaltered raw Optos P200dTx and Zeiss Clarus images.

Image Registration

We realized that the two images of the same retinal location in the same eye acquired from these two fundus cameras cannot be used directly for any comparative study, as they were acquired at different angles, using different focal lengths and zoom factors, as well as viewpoints. In order to facilitate comparison, we decided to adjust the scaling, rotation, and skewing of an image from one camera to transform it to match the coordinate system of the image from the other camera. This process of aligning one image with respect to another is referred to as image registration.⁸ Ryan et al.⁹ presented a method to register a pair of retinal images using control points whose matching is not known. They computed similarity transformation coefficients and then employed the expectation maximization algorithm before achieving registration. Recently, Hernandez-Matas et al.¹⁰ proposed retinal image registration as a tool to support clinical applications. They studied eye shape

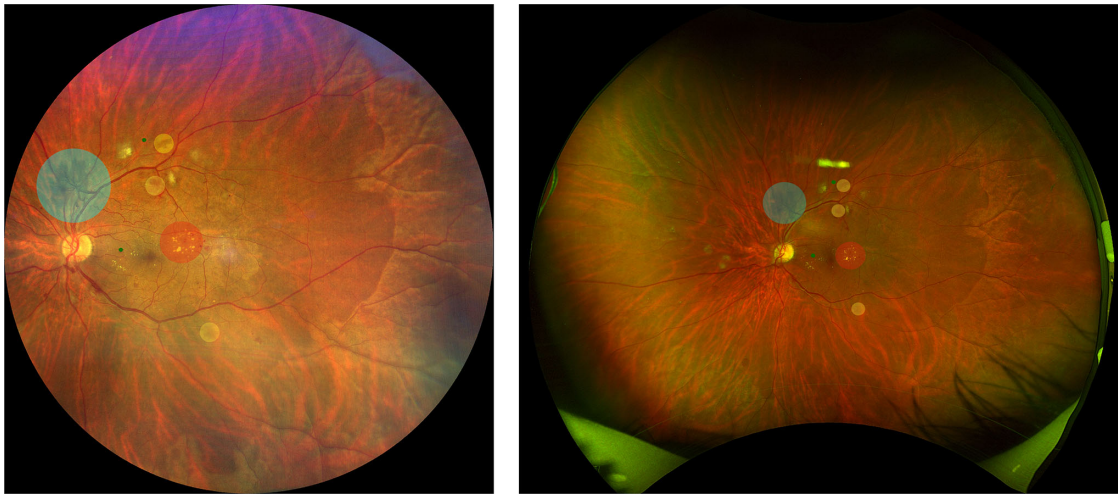


Figure 1. Retinal fundus images of “patient x,” obtained by the Zeiss Clarus 500 device (left) and the Optos P200dTx device (right), were professionally graded for lesions. The *large blue circle* denotes neovascularization elsewhere; the *medium red circle* denotes hard exudates; the *small yellow circle* denotes hemorrhages; and the *green point* denotes microaneurysms.

estimations that can improve the measurements that affect clinicians’ diagnoses by allowing measurements on three-dimensional models rather than on two-dimensional images with projection distortion. In this study, we performed manual registration of images. This involved selection of control (key) points, the landmarks that can be clearly observed on both images (e.g., first-order branching of vessels). This was followed by creation of a transformation matrix on the basis of control points followed by application of the transformation to the input images. Control point registration was performed using MATLAB R2020b (MathWorks, Natick, MA) on a batch of input image pairs (Optos P200dTx and Zeiss Clarus 500). Two pairs of points were chosen as control points for a pair of input images, and non-reflective similarity transformation was employed. Non-reflective similarity, a subset of affine transformations, may include rotation, scaling, and translation while preserving shapes and angles, as well as keeping straight lines and parallel lines straight and parallel, respectively. The results of the transformation were computed and stored in a file, and a superimposed image of both the Zeiss Clarus 500 and Optos P200dTx was created, as shown in Figure 2. The approximate time to register one pair of images was on the order of a few seconds. More time was required for accurate selection of the control point pairs compared with the actual registration. In total, 385 Optos P200dTx and Zeiss Clarus 500 images were registered and constructed with this method. After registration, the images had identical resolution (4000 × 4000 pixels), with the key points in both images aligned as seen in the bottom image of Figure 2.

Spatial Localization of a Lesion

To analyze the spatial localization of lesions, we divided the superimposed retinal image into three regions, with the optic disc as the reference point. As shown in Figure 3, the three regions or zones (namely, C1, C2, and C3) were projected over the superimposed image constructed, representing the central, mid-peripheral, and peripheral retina, respectively. Zone C1 (central retina) referred to a circular region with a maximum distance of 500 pixels from the optic disc; zone C2 (mid-peripheral retina) was defined as a region with a distance measuring more than 500 but less than 1000 pixels from the optic disc; and the region with a distance of at least 1000 pixels or more from the optic disc was zone C3 (peripheral retina).

Localization of Lesions Present in Both the Optos P200dTx and Zeiss Clarus 500

Every lesion was associated with an assigned weight based on its type or size as described earlier. For example, point-type lesions such as MA were each associated with a weight of one, whereas a larger lesion marked by a circular region was assigned a larger value of weight based on its marked area.

The number of lesions of a specific type k in an image (Im), denoted by $n^k(Im)$, was computed by the summation of the weights of all of the lesions:

$$n^k(Im) = \sum_{\text{Type } k \text{ lesions: } ls \in Im} \text{weight}(ls) \quad (1)$$

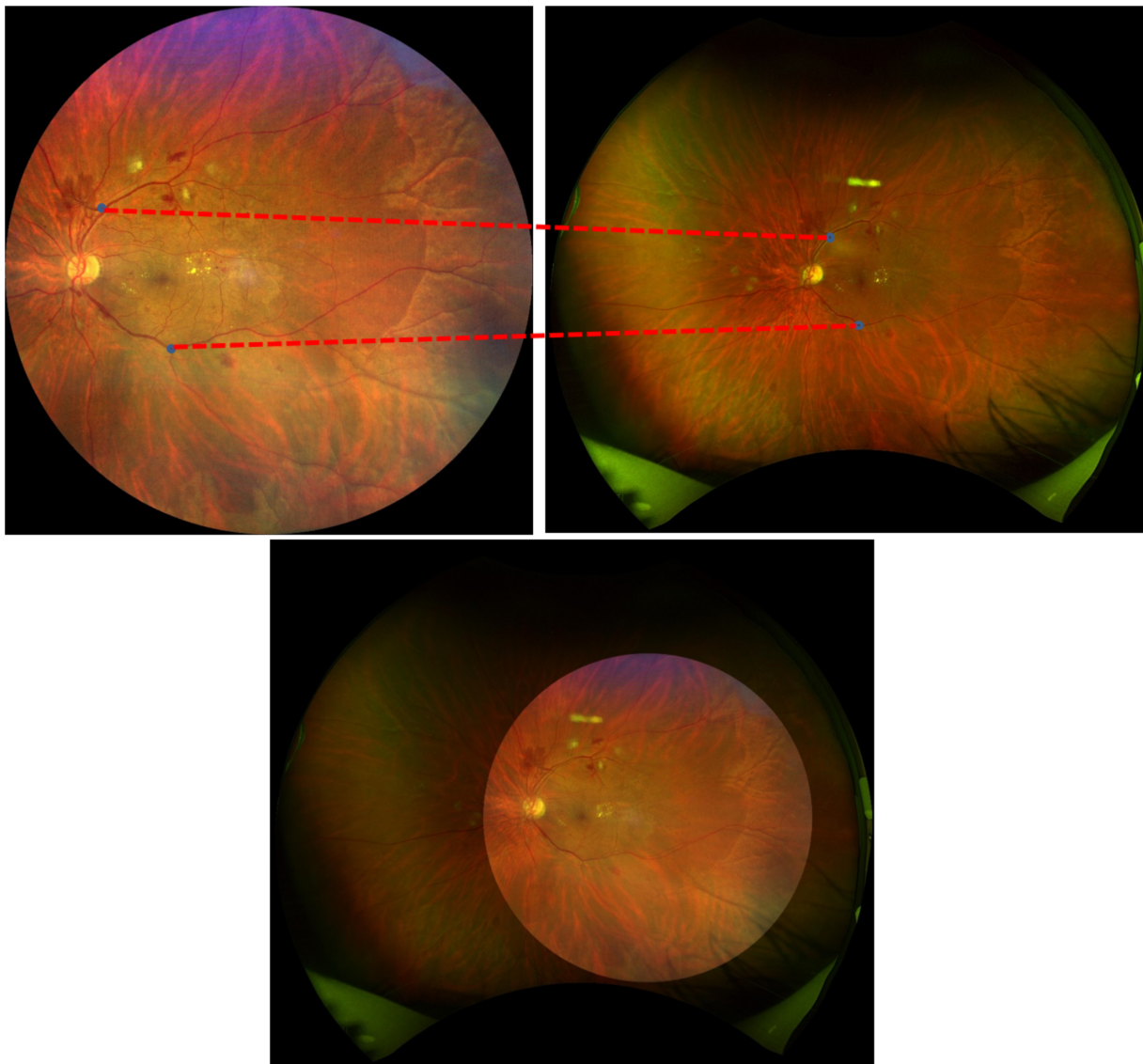


Figure 2. An example of Optos P200dTx–Zeiss Clarus 500 image registration. The top row shows two retinal images of the same “patient x” captured by the Zeiss Clarus 500 (left) and the Optos P200dTx (right). Two small blue circles on each of them shows the two branching points chosen as the control points. The red dashed line shows the correspondence of each of the control points. Images in the bottom row show the blended version of the Optos P200dTx and Zeiss Clarus 500 images after registration.

For a given Optos P200dTx–Zeiss Clarus 500 pair, to identify the corresponding lesion ls_o^k of type k in the Optos P200dTx, for a given lesion ls_c^k of type k occurring in the Zeiss Clarus 500 image we sorted the distance between ls_c^k and every lesion in the Optos P200dTx in an increasing order using the Euclidean distance metric, and the first lesion in the sorted list became a likely candidate for ls_o^k . Four categories of lesion comparisons are possible for a registered image pair: point versus point (category 1), point versus region (category 2), region versus point (category 3), and region versus region (category 4). Based on the

markings for each lesion type as discussed earlier, we employed different markers for lesion comparisons. MA was marked using a point; hence, only category 1 was used for MA lesion comparisons. CWS and VH were marked using small-sized regions; hence, for both CWS and VH, category 4 was employed. All other lesions were marked by point or small- or medium-sized regions; hence, for their lesion comparisons, all four categories were employed.

To handle slight variations in terms of pixel coordinates in identifying the same lesions in both images of the Optos P200dTx–Zeiss Clarus 500 pair, we

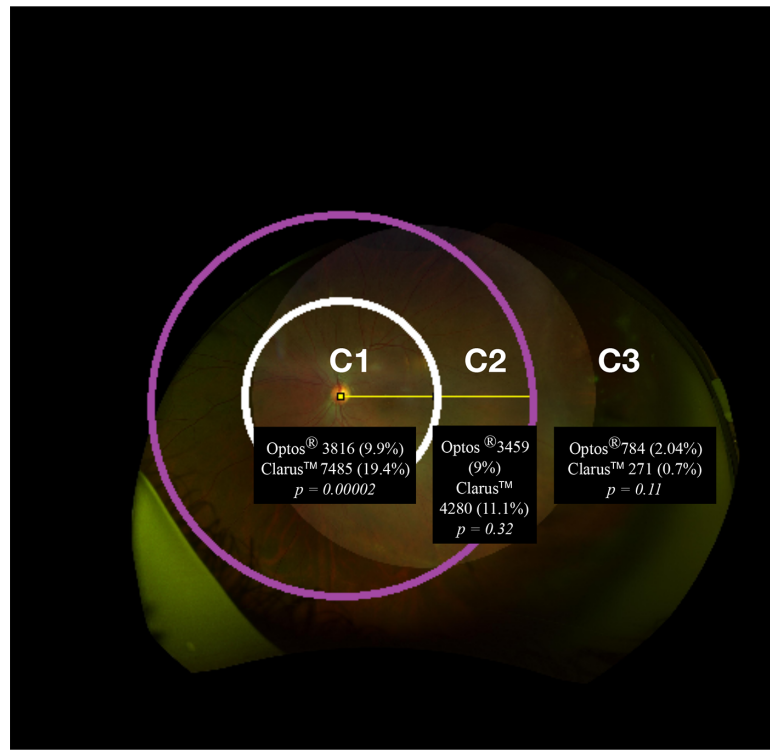


Figure 3. An illustrative example of DR lesions detected by the Zeiss Clarus 500 and by the Optos P200dTx with respect to the blended superimposed images spatially delineated as C1 (central retina), C2 (mid-peripheral retina), and C3 (peripheral retina). Similar zonal segregation of the retina was performed on the superimposed images of all patients. Differences in the number of lesions identified within each zone by each device and their statistical significance are noted.

introduced different threshold values in terms of number of pixels for each of the above categories. When the grader annotated a point-wise lesion, there was some potential for error in the process of exactly localizing the coordinates as compared with marking a circular region over the lesions concentrated in that area. Thus, we employed a higher threshold of 20 pixels for comparing point-type lesions (category 1) as compared with a threshold of 10 pixels for point-type and area-type lesions (category 2 and 3) and a threshold of 5 pixels for two area-type lesions (category 4). The threshold value of 20 pixels for point-versus-point lesion comparisons (category 1) was obtained by computing the mean difference between optic disc centers marked by the graders in both images (registered with respect to the Optos P200dTx image).

To compute the number of lesions of type k ($0 < k < 7$) captured by the Zeiss Clarus 500 but missed by the Optos P200dTx, the weights were gradually reduced in both the images for the lesions where correspondence was established in both the images. The remaining weights of Zeiss Clarus 500 lesions (type k) gave the number of type k lesions that were captured by the Zeiss Clarus 500 but missed by the Optos P200dTx.

Similar procedure was repeated to compute the number of lesions of type k captured by the Optos P200dTx but missed by the Zeiss Clarus 500.

For a lesion ls_c^k in the Zeiss Clarus 500, when its corresponding lesion ls_o^k had been found in the Optos P200dTx image, the weights of both ls_c^k and ls_o^k were reduced by 1 if at least one of them was a point-type lesion (categories 1, 2, and 3). When comparing two lesions belonging to category 4 in both the Optos P200dTx and Zeiss Clarus 500, the common area of intersection was computed between the two regions and accordingly the weights of both ls_c^k and ls_o^k were reduced.

When the same procedure had been repeated for all such lesions ls_c^k of type k in the Zeiss Clarus 500, Equation 1 was recomputed to obtain the summation of the remaining weights for all lesions ls_c^k that gave the number of lesions of type k captured by the Zeiss Clarus 500 but missed by the Optos P200dTx. Similar count values were obtained for Optos P200dTx images that were missed by the Zeiss Clarus 500. If $n^k(I_{cla}, I_{opt})$ denotes the number of lesions of type k found in both images (I_{opt} and I_{cla}) of an Optos P200dTx-Zeiss Clarus 500 pair, we computed the

number of lesions missed in the Optos P200dTx as $m^k(I_{opt})$, where

$$m^k(I_{opt}) = n^k(I_{cla}) - n^k(I_{cla}, I_{opt}) \quad (2)$$

Similarly, the number of lesions missed in the Zeiss Clarus 500 was computed by the following equation:

$$m^k(I_{cla}) = n^k(I_{opt}) - n^k(I_{cla}, I_{opt}) \quad (3)$$

Statistical Analysis

All of the image analyses were performed by developing scripts using the Python programming language.

Further statistical analyses were performed using SPSS Statistics 21.0 (IBM, Armonk, NY). Table 1 provides the demographic data for our patient sample; continuous variables are represented in terms of mean and standard deviation and were compared using Student's *t*-test. Similarly, demographic variables comprised of categorical data are presented as a number and percentage and were compared using the χ^2 test. In Tables 2 and 3, the χ^2 test was performed to compare the distribution of lesions missed across the two cameras with respect to size, color, and varying regions within the retina. Finally, a multivariate logistic regression was performed to compare the two cameras, with identification of DR lesions as the primary outcome. The *P* values of the significance tests for each set

Table 1. Baseline Characteristics of the Study Population

Variables	Absence of DR Lesion (<i>n</i> = 117)	Presence of DR Lesion (<i>n</i> = 268)	<i>P</i>
Age (yr), mean \pm SD	54.08 \pm 9.70	56.96 \pm 9.18	0.006
Male gender, <i>n</i> (%)	79 (67.50)	187 (69.80)	<0.0001
Systemic diseases, <i>n</i> (%)			
Duration of diabetes (yr), mean \pm SD	7.87 \pm 4.54	12.16 \pm 7.30	<0.0001
Hypertension	24 (20.50)	92 (34.30)	<0.0001
Cardiovascular disease	4 (3.40)	17 (6.30)	0.005
Dyslipidemia	6 (5.10)	28 (10.40)	<0.0001
Chronic kidney disease	4 (3.40)	4 (1.50)	1.000
Lens status, <i>n</i> (%)			
Clear	74 (63.20)	94 (35.10)	0.123
Immature cataract	20 (17.10)	108 (40.30)	<0.0001
Pseudophakia	21 (17.90)	62 (23.10)	<0.0001
Aphaki	2 (1.70)	4 (1.50)	0.414
Clinical diagnosis, <i>n</i> (%)			
Mild NPDR	0 (0.00)	7 (2.61)	0.078
Moderate NPDR	1 (0.90)	39 (14.55)	0.0001
PDR	0 (0.00)	69 (25.75)	<0.0001
No DR	55 (47.00)	63 (23.50)	0.461
Spherical equivalent of refractive error, mean \pm SD	-0.82 \pm 4.31	-0.48 \pm 3.94	0.439

Table 2. Percentage of Lesions Missed by Optos P200dTx and Zeiss Clarus 500 in Each of the Regions C1, C2, and C3

Lesions	C1			C2			C3		
	Missed by Clarus 500, <i>n</i> (%)	Missed by P200dTx, <i>n</i> (%)	<i>P</i>	Missed by Clarus 500, <i>n</i> (%)	Missed by P200dTx, <i>n</i> (%)	<i>P</i>	Missed by Clarus 500, <i>n</i> (%)	Missed by P200dTx, <i>n</i> (%)	<i>P</i>
MA	11 (10)	38 (34.55)	<0.0001	30 (28.30)	34 (32.08)	0.254	14 (73.68)	3 (15.79)	<0.0001
RH	19 (14.18)	37 (27.61)	<0.0001	19 (14.18)	35 (26.12)	<0.0001	30 (57.69)	8 (15.38)	<0.0001
HE	12 (9.16)	37 (28.24)	<0.0001	19 (22.09)	26 (30.23)	0.010	16 (76.19)	2 (9.52)	<0.0001
CWS	3 (10.71)	18 (64.29)	<0.0001	4 (23.53)	10 (58.82)	<0.0001	1 (50.00)	0 (0.00)	<0.0001
NVE	16 (32.00)	21 (42.00)	0.004	9 (18.75)	23 (47.92)	<0.0001	2 (28.57)	4 (57.14)	<0.0001
NVD	1 (6.00)	5 (29.00)	<0.0001	NA	NA	NA	NA	NA	NA
SHH	28 (25.45)	21 (19.09)	0.024	33 (31.13)	31 (29.25)	0.570	12 (63.16)	5 (26.32)	<0.0001
VH ^a	7 (38.89)	8 (44.44)	0.118	8 (61.54)	3 (23.08)	<0.0001	7 (63.64)	3 (27.27)	<0.0001

Bold values are statistically significant.

^aEach set of the eight comparison *P* values is Bonferroni corrected (Bonferroni corrected *P* < 0.002).

Table 3. Distribution of Missed Lesions by Zeiss Clarus 500 and Optos P200dTx Based on the Color and Size of the Lesions

Lesions	Missed by Clarus 500, n (%)	Missed by P200dTx, n (%)	P
Lesion color			
Red MA, RH, NVE, NVD, SHH, VH	246 (25.79)	279 (29.25)	0.091
Yellow HE	47 (19.75)	65 (27.31)	0.052
White CWS	8 (17.02)	28 (59.57)	<0.0001
Lesion size			
Small MA, RH, NVE, NVD	151 (22.30)	208 (30.72)	0.0005
Medium HE, CWS	55 (19.30)	93 (32.63)	0.0003
Large SHH, VH	95 (34.30)	71 (25.63)	0.056

Bold values are statistically significant.

of contrasts among the three groups for each of the eight measures were adjusted for multiple comparisons using the Bonferroni technique, yielding a two-tailed alpha of $0.05/(3 \times 8)$. Fleiss' unweighted kappa, a statistical measure for assessing the reliability of agreement among multiple observers when assigning categorical ratings to a number of items or classifying items, was utilized. $P < 0.05$ was considered statistically significant.

Results

Patient Characteristics and Baseline Demographics of the Study Sample

A total of 243 patients with prior clinical diagnosis of type 2 diabetes were recruited based on inclusion and exclusion criteria and underwent clinical retinal eye examination, along with collection of fundal imagery using both cameras. A total of 385 fundus pictures were obtained for the grading, out of which 101 were unilateral eyes and 142 were bilateral eyes.

Table 1 provides the baseline characteristics of the patients based on the presence or absence of DR lesions. Of 385 fundus pictures, 268 images were detected with varying grades of DR (69.61%), and 117 images were detected with no DR (30.39%). In addition, statistically significant increases in patients with moderate non-proliferative diabetic retinopathy (NPDR) and proliferative diabetic retinopathy (PDR) were noted in the group with a presence of DR lesions. Age, duration of diabetes mellitus, presence of hypertension, cardiovascular disease, dyslipidemia, chronic kidney disease, presence of immature cataract, and pseudophakic eyes were noted to be significantly increased in the group with a presence of DR lesions ($P < 0.05$).

Statistical Results Involving Interobserver Agreement and Non-Independence of Samples

To ensure non-violation of the independence of samples regarding bilateral eye images from the same patient, the odds ratio from the two-eye analysis, with inter-eye correlation adjusted using the generalized linear mixed model, generalized estimating equation with a working independence correlation matrix, and a compound symmetry correlation matrix, was 4.609 (95% confidence interval [CI], 2.608–6.661; $P = 0.0005$) for DR lesions. No statistically significant correlation between images was noted; hence, independence of the sample images was preserved.

To check for interobserver variation, Fleiss κ measures were utilized to ensure adequate validity. For red color lesions (MA, RH, NVE, NVD, SHH, and VH), κ among the 10 graders was moderate ($\kappa = 0.50$); for yellow color lesions (HE), κ was also moderate ($\kappa = 0.50$); and κ for white color lesions (CWS) was fair ($\kappa = 0.31$).

Comparison of Lesion Detection Between Both Cameras

Figure 3 shows the distribution of pathological lesions in zones C1, C2, and C3 detected by the Optos P200dTx versus the Zeiss Clarus 500. In zone C1, a statistically significant greater number of lesions were identified by the Zeiss Clarus 500 (19.4%) than by the Optos P200dTx (9.9%) ($P = 0.0002$) when compared against total lesions identified in the retina. In zone C2, the Zeiss Clarus 500 was once again able to detect more lesions (11.1%) than the Optos P200dTx (9%); however, in zone C3, the Optos P200dTx had a higher detection rate (2.04%) than the Zeiss Clarus (0.7%). These findings for zones C2 and C3 were not noted to be statistically significant.

Supplementary Table S1 shows the distribution of images based on the detection of lesions captured by both cameras. For every lesion type, the number of Zeiss Clarus 500 images having at least one lesion of that type was compared with the number of Optos P200dTx images having at least one lesion of the same type. The results, shown in Supplementary Table S1, indicated that the image level agreement varied from 16.7% for SHH to 65.6% for RH.

Supplementary Table S2 compares the distribution of lesions identified by the two cameras based on zones C1, C2, and C3. Within zone C1, although there was no statistically significant difference in identification of NVE and NVD between the two cameras, detection of the remaining six lesions by the Zeiss Clarus 500 compared with the Optos P200dTx was noted to be statistically significant ($P < 0.0001$, after Bonferroni adjustment). Within zone C2, the identification of MA, HE, and VH were noted to be significantly greater for the Optos P200dTx than the Zeiss Clarus 500 ($P < 0.0001$, after Bonferroni adjustment). Within zone C3, all of the DR lesions except CWS, NVD, and VH were identified at a significantly greater rate for the Optos P200dTx than the Zeiss Clarus 500 ($P < 0.0001$, after Bonferroni adjustment).

Table 2 shows the percentage of lesions missed by the Optos P200dTx and those by the Zeiss Clarus 500 in each of the regions (C1, C2, and C3) for each lesion type. In C1, frequently missed lesions by the Zeiss Clarus 500 included VH (38.9%) and those by Optos P200dTx included CWS (64.3%) and NVE (42.0%) ($P < 0.0001$, after Bonferroni adjustment). In C2, Zeiss Clarus 500 imaging missed VH (61.5%) and SHH (31.3%); whereas, the Optos P200dTx missed CWS (58.8%) and NVE (47.9%) ($P < 0.0001$, after Bonferroni adjustment). In C3, the frequently missed lesions by the Zeiss Clarus 500 included HE (76.2%) and MA (73.7%), and lesions frequently missed by the Optos P200dTx included NVE (57.1%) ($P < 0.0001$, after Bonferroni adjustment).

Table 3 shows the distribution of missed lesions on the Zeiss Clarus 500 and Optos P200dTx based on the color and size of the lesions. More white lesions were missed by the Optos P200dTx (59.57%) as compared with the Zeiss Clarus 500 (17%) ($P < 0.0001$). Likewise, more small and medium lesions were missed by the Optos P200dTx (30.72% and 32.63%, respectively) than by the Zeiss Clarus 500 (22.30% and 19.30%, respectively) ($P < 0.05$).

Multivariate Analysis

Table 4 shows the multivariate regression model with respect to overall detection of DR lesions. The

Table 4. Multivariate Logistic Regression Model Representing the Detection of Diabetic Retinopathy Lesions as the Outcome

Variable	Regression Coefficient	P
Overall Clarus 500 lesions	1.89	0.91
Overall P200dTx lesions	0.96	0.94
Age (yr)	0.02	1.00
Duration of diabetes (yr)	0.30	0.99
Male gender	-1.91	1.00
Hypertension	-0.52	1.00
Heart disease	-141.32	0.97
Cholesterol	-6.83	1.00
Lens status		
Clear	—	1.00
Immature cataract	-8.53	0.99
Pseudophakia	-3.97	1.00
Aphakia	-8.41	1.00

Adjusted $R^2 = 0.520$; $P < 0.05$.

regression coefficient for the detection of DR lesions when compared with clinically diagnosed lesions was found to be higher overall in the Zeiss Clarus 500 (21.49) when compared with the Optos P200dTx (9.78). However, this difference, although clinically significant, was not found to be statistically significant.

Discussion

Identification of retinal lesions is critically important in DR where detailed and accurate recognition of the lesion types and location is essential in order to grade disease severity.¹¹ Only a few researchers have previously compared UWF imaging devices. A study done by Hirano et al.¹² showed that, in a single capture, the Optos P200dTx camera captured 465 disc areas and the Zeiss Clarus 500 captured up to 243 disc areas. The authors also found higher DR severity for Zeiss Clarus 500 images than for Optos P200dTx images, as well as a larger volume of peripheral retinal lesions in the Optos P200dTx images. However, no mention was made of which lesions were particularly missed by either camera,¹² which has been addressed by our study.

Another study by Witmer et al.¹³ found that the Optos P200dTx captured greater temporal and nasal retinal surface pixel areas, whereas the Heidelberg Spectralis HRA+OCT captured more superior and inferior retinal vasculature. Chen et al.¹⁴ reported that the Optos P200dTx consistently captured more relative pixels in all four quadrants compared with the Zeiss Clarus 500. All of these studies compared the area of retina captured by the cameras but none of them

reported the accuracy of lesion identification for the different devices. Although UWF cameras have proven to be an effective tool for screening and documentation of various retinal pathologies in recent years, what we can infer from the prior literature is that there is a need to generate an optimal imaging system that can accurately detect peripheral and central field lesions, but such a device is not yet available. In the meantime, the choice of which UWF camera to use is best based on clinician preference and patient disease presentation and characteristics.

Of note, a study done by Sears et al.⁴ reported that, compared with Indian eyes, Caucasian eyes have more DR lesions scattered at the periphery. This shows that there might be an ethnic variation in the distribution of lesions especially involving the periphery. Hence, our present study compares two of the UWF cameras widely used in the clinical setting, Optos P200dTx and Zeiss Clarus 500, with respect to the detection of DR lesions within a primarily South Asian cohort.

Based on our study, which utilized two UWF cameras, we found that 56.5% of lesions were detected in zone C1, 38.5% were detected in zone C2, and 5.3% were detected in zone C3. These results show that a primarily South Asian population tends to present with primarily center-involving lesions and those presenting in the peripheral retina are limited, as confirmed by the study results of Sears et al.⁴ In our study, eight types of lesions were considered for annotation to generate the ground truth: microaneurysm, retinal hemorrhage, hard exudates, cotton wool swab, neovascularization in disc, neovascularization elsewhere, subhyaloid hemorrhage, and vitreous hemorrhage. When comparing the two UWF imaging cameras with respect to single-field images using an overall image level, we found that the sight-threatening lesions such as NVE and NVD were detected equally by both cameras in zone C1, whereas other lesions were identified better by the Zeiss Clarus 500 in zone C1. When we looked at how many lesions were missed by either of the cameras, we found that the Optos P200dTx missed almost 50% of the lesions found by the Zeiss Clarus 500 in zone C1. In zone C2, however, both cameras could identify almost the same number of images; the Zeiss Clarus 500 definitely fared better in terms of clarity and ease of identification. In zone C3, the Zeiss Clarus 500 missed around 7% of the lesions identified by the Optos P200dTx. Hence, the utility of the Zeiss Clarus 500 device versus the Optos P200dTx can be greater in populations presenting with a higher prevalence of retinal lesions confined to zone C1, as noted in our sample cohort.

Neovascular age-related macular degeneration (AMD) is a condition that occurs mostly in the posterior pole. Maruyama et al.¹⁵ found that the Zeiss Clarus

500 was superior to the Optos P200dTx for identifying neovascular AMD with high sensitivity and specificity because of its ability to image high-resolution widefield fundus, true color imaging, and good resolution. The authors reported that, in neovascular AMD, the Zeiss Clarus 500 can detect smaller lesions in the posterior pole better than the Optos P200dTx. Similarly, most diabetic retinopathy lesions in our sample were localized to zones C1 and C2 (posterior pole), where the Zeiss Clarus 500 offered better detection than the Optos P200dTx.

According to Kumar et al.,¹⁶ the lower sensitivity of the Zeiss Clarus 500 in the temporal quadrant could be attributed to a smaller field of vision acquired in the temporal quadrant as a result of a patient's nose interfering with rotating the body of the camera to capture images in the extreme temporal periphery. Similarly, in our study, the Optos P200dTx detected peripheral lesions in zone C3 better than the Zeiss Clarus 500.

No statistical significance in the overall identification of DR lesions was found when we performed multivariate analyses. However, based on clinical significance, an overall greater number of lesions was identified by the Zeiss Clarus 500 compared with the Optos P200dTx when compared against clinically diagnosed DR lesions. To explain these findings, we must first consider eyelashes as being important image artifacts in such images. In the Optos P200dTx images, a patient's lashes often blocked the inferior portions of the retinal image.¹⁷ The Zeiss Clarus 500, on the other hand, employs partial confocal scanning optics,¹³ essentially eliminating eyelid and eyelash artifacts. This can be a disadvantage in terms of obscuring images of the peripheral retina. Second, the depth of focus is wider for the Optos P200dTx due to its confocal scanning laser ophthalmoscope system with an ellipsoidal mirror. This difference in depth of focus was thought to be one of the reasons why peripheral retinal blood vessels appeared clearer in the Optos P200dTx images than in the Zeiss Clarus 500 images, especially in the temporal retina. Another factor is different locations for the center of the images. In the Optos P200dTx, the center of the image corresponds to the fovea, whereas in a montage image from the Zeiss Clarus 500, the center of the image lies slightly nasal to the fovea. Stereographic projection software built into the Optos P200dTx solves the problems of peripheral distortion in a predictable manner by projecting peripheral lesions in corrected physical dimensions¹⁸; however, this did not play a significant role in this study because the primary objective was to identify the lesions rather than to precisely quantify them. When looking at lesions detected in zone C3, more lesions were detected by the Optos P200dTx, as it captures a

wider field of view in a single image.¹⁹ The lesser sensitivity of the Zeiss Clarus 500 in the temporal quadrant in this study is likely due to a lesser field of view for single images acquired in the temporal quadrant.

When comparing the detection of DR lesions based on color in all regions of the retina, we found that more lesions were missed by the Optos P200dTx than the Zeiss Clarus 500 for all three colors (red, yellow, and white); however, the increase in missed white lesions (cotton wool spots) by the Optos P200dTx was found to be significant. Likewise, there was a larger tendency of missing smaller lesions with the Optos P200dTx. These findings could be due to the Optos P200dTx utilizing pseudocolor imaging with a resolution of 14 to 20 µm when compared with the Zeiss Clarus 500, which utilizes true color imaging with a resolution of 7 µm.¹⁹ Additionally, the issues with identification of lesions anterior to the retina, such as vitreous hemorrhage, could be due to the technique of imaging, as the photographer aims to focus on the posterior pole, as well as by the fact that the Optos P200dTx captures the image as soon as the posterior pole is clearly imaged on the sensor.

Our study had a few limitations. Multiple graders had different perspectives of views while grading the Optos P200dTx and Zeiss Clarus 500 images; thus, the selection of circles for marking larger or groups of lesions with medium or larger circles would have differed, resulting in intergrader bias. A single capture of the Zeiss Clarus 500 was never intended to image the same extent of peripheral retina as the Optos P200dTx; thus, it is difficult to use these results to evaluate the ability of each device to image the peripheral retina. The UWF systems are meant to image fundus with a non-mydriatic pupil. The minimum pupil diameters required to capture images on the Optos P200dTx and Zeiss Clarus 500 are 2 mm and 2.5 mm, respectively. However, all patients included in our study had dilated pupils. This could have improved the quality of the images, making imaging easier than it would have been in the case of a non-mydriatic pupil. The thresholds to detect differences between the cameras were 20 pixels for point lesions and 10 and 5 pixels for the regions. Changing the thresholds could change the results. For the registrations of the images, only two branching points were employed, although choosing more correspondence points for an Optos P200dTx–Zeiss Clarus 500 image pair could improve the image registration.

Conclusions

Although our study found that both instruments were good in identifying sight-threatening DR, early

lesions of DR, which are important from a screening point of view, can be missed if the resolution is low. This becomes more important in a South Asian population where peripheral changes in DR are smaller. However, further studies are needed to ascertain if higher resolution is better for screening and wider view cameras are better for deciding the management plans in diabetic retinopathy. Prospective studies with a large sample size and comparing varying ethnic groups are required to further evaluate the utility of both the UWF cameras in eyes with different lenticular and refractive status and also to assess if the differences in the retinas imaged are clinically significant in different disease states.

Acknowledgments

The authors thank the graders of the diabetic retinopathy project team: G. Kumar, K.R. Loheshwari, S. Mathangi, P. Gaurav, S. Sowmya, S. Ramya, S.D. Chitralekha, M.N. Swathi Priya, B. Gnanapoonkodi, and K. Meenakshi.

Disclosure: R. Khan, None; S. Raman, None; S.K.M. Karamchetti, None; S. Srinivasan, None; A. Sharma, None; J. Surya, None; M. Bhende, None; K. Ramasamy, None; A. Verma, None; R. Raman, None

References

1. Tabish SA. Is diabetes becoming the biggest epidemic of the twenty-first century? *Int J Health Sci (Qassim)*. 2007;1(2):V–VIII.
2. Early Treatment Diabetic Retinopathy Study Research Group. Grading diabetic retinopathy from stereoscopic colour fundus photographs—an extension of the modified Airlie House classification: ETDRS report number 10. *Ophthalmology*. 1991;98(5 suppl):786–806.
3. Aiello LP, Odia I, Glassman AR, et al. Comparison of early treatment diabetic retinopathy study standard 7-field imaging with ultrawide-field imaging for determining severity of diabetic retinopathy. *JAMA Ophthalmol*. 2019;137(1):65–73.
4. Sears CM, Hirano T, Nittala MG, et al. Ethnic variation in diabetic retinopathy lesion distribution. *Invest Ophthalmol Vis Sci*. 2018;59(9):4681.
5. Silva PS, Cavallerano JD, Haddad NM, et al. Peripheral lesions identified on ultrawide field

- imaging predict increased risk of diabetic retinopathy progression over 4 years. *Ophthalmology*. 2015;122(5):949–956.
- 6. Diabetic Retinopathy Clinical Research Network. Peripheral diabetic retinopathy (DR) lesions on ultrawide-field fundus images and risk of DR worsening over time. Available at: <https://public.jaeb.org/drcrnet/stdy/239>. Accessed September 21, 2021.
 - 7. Patel SN, Shi A, Wibbelsman TD, Klufas MA. Ultra-widefield retinal imaging: an update on recent advances. *Ther Adv Ophthalmol*. 2020;12:2515841419899495.
 - 8. Alam F, Rahman SU. Challenges and solutions in multimodal medical image subregion detection and registration. *J Med Imaging Radiat Sci*. 2019;50(1):24–30.
 - 9. Ryan N, Heneghan C, de Chazal P. Registration of digital retinal images using landmark correspondence by expectation maximization. *Image Vis Comput*. 2004;22(11):883–898.
 - 10. Hernandez-Matas C, Zabulis X, Argyros AA. Retinal image registration as a tool for supporting clinical applications. *Comput Methods Programs Biomed*. 2021;199:105900.
 - 11. Duh EJ, Sun JK, Stitt AW. Diabetic retinopathy: current understanding, mechanisms, and treatment strategies. *JCI Insight*. 2017;2(14):e93751.
 - 12. Hirano T, Imai A, Kasamatsu H, Kakihara S, Toriyama Y, Murata T. Assessment of diabetic retinopathy using two ultra-wide-field fundus imaging systems, the Clarus and Optos systems. *BMC Ophthalmol*. 2018;18(1):1–7.
 - 13. Witmer MT, Parlitsis G, Patel S, Kiss S. Comparison of ultra-widefield fluorescein angiography with the Heidelberg Spectralis noncontact ultra-widefield module versus the Optos Optomap. *Clin Ophthalmol*. 2013;7:389–394.
 - 14. Chen A, Dang S, Chung MM, et al. Quantitative comparison of fundus images by 2 ultra-widefield fundus cameras. *Ophthalmol Retina*. 2021;5(5):450–457.
 - 15. Maruyama-Inoue M, Kitajima Y, Mohamed S, et al. Sensitivity and specificity of high-resolution wide field fundus imaging for detecting neovascular age-related macular degeneration. *PLoS One*. 2020;15(8):e0238072.
 - 16. Kumar J, Kohli P, Babu N, Krishnakumar K, Arthur D, Ramasamy K. Comparison of two ultra-widefield imaging for detecting peripheral retinal breaks requiring treatment. *Graefes Arch Clin Exp Ophthalmol*. 2021;259(6):1427–1434.
 - 17. Verma A, Alagorie AR, Ramasamy K, et al. Distribution of peripheral lesions identified by mydriatic ultra-wide field fundus imaging in diabetic retinopathy. *Graefes Arch Clin Exp Ophthalmol*. 2020;258(4):725–733.
 - 18. Tan CS, Chew MC, van Hemert J, Singer MA, Bell D, Sadda SR. Measuring the precise area of peripheral retinal non-perfusion using ultra-widefield imaging and its correlation with the ischaemic index. *Br J Ophthalmol*. 2016;100(2):235–239.
 - 19. Matsui Y, Ichio A, Sugawara A, et al. Comparisons of effective fields of two ultra-widefield ophthalmoscopes, Optos 200Tx and Clarus 500. *Biomed Res Int*. 2019;2019:7436293.